https://doi.org/10.5194/acp-2019-1156
Preprint. Discussion started: 6 February 2020

Atmospheric Chemistry and Physics Discussions

Laboratory studies of fresh and aged biomass burning aerosols emitted from east African biomass fuels-PART 1-Optical properties

Damon M. Smith,[1,2,#] Marc N. Fiddler[3], Rudra Pokhrel[1], Solomon Bililign[1*]

1. Department of Physics, North Carolina Agricultural and Technical State University, Greensboro, NC, 27411 USA,
2. Applied Sciences and Technology Program, North Carolina A&T State University, Greensboro, NC 27411, USA,
3. Department of Chemistry, North Carolina Agricultural and Technical State University, Greensboro, NC, 27411, USA

Current address: Department of Chemistry and Physics, Western Carolina University, Cullowhee, NC 28723
* Correspondence: Bililignsol@gmail.com; Tel.: (+13362852328);

Abstract: An accurate measurement of optical properties of aerosols is critical for quantifying the effect of aerosols on climate. Uncertainties persist and measurement results vary significantly. Biomass burning (BB) aerosols have been extensively studied through both field and laboratory environments for North American fuels to understand the changes in optical and chemical properties as a function of aging. There is a clear research need for a wider sampling of fuels from different regions of the world for laboratory studies. This work represents the first such study the optical and chemical properties of three wood fuel samples used commonly for domestic use in east Africa. In general, combustion temperature plays a major role on the optical properties of the emitted aerosols. For fuels combusted at 800^{o} C single scattering albedo (SSA) values are in the range between 0.287 and 0.439 while the SSA for fuels combusted at 500^{o} C, the range between 0.66 and 0.769. There is a clear but very small dependence of SSA on fuel type, with eucalyptus producing aerosol with higher SSA than olive and acacia. A significant increase in the scattering and extinction cross-section (mostly dominated by scattering) was observed, indicating the occurrence of chemistry, even during dark aging for combustion at 500^{o} C. This fact cannot be explained by the heterogeneous chemistry and we hypothesized secondary organic aerosol formation as a potential phenomenon happing during dark aging. After 12 h of photochemical aging, BB aerosol becomes highly scattering with SSA values above 0.9, which can be attributed to oxidation in the chamber. Due to the very low number concentration of aerosols during aging studies of combustion at 800^{o} C, the results were inconclusive. We also attempted to simulate polluted urban environments by ejecting volatile organic compounds (VOCs) and BB aerosol into the chamber, but no distinct difference was observed, since measurements were done 12 hours after injection of VOCs.

1 Introduction

The role of biomass burning (BB) aerosols on air quality, human health, cloud formation, and climate remain poorly quantified. BB aerosol play an important role in the earth's radiation budget and in the hydrological cycle by absorbing and scattering sunlight and by providing nuclei for cloud condensation (Crutzen and Andreae, 1991). There has been several estimates of the radiative forcing of BB aerosols ranging from 0.03 ± 0.12 W m^{2} (Forster et al., 2007)

https://doi.org/10.5194/acp-2019-1156
Preprint. Discussion started: 6 February 2020

Atmospheric Chemistry and Physics Discussions

to the most recent estimate of −0.2 W m^{-2} (Boucher, 2013). The uncertainty associated with the radiative forcing, is in the range of –0.07 to –0.6 W m^{-2} (IPCC, 2014). This high level of uncertainty is associated with uncertainty in measuring of the optical properties of BB aerosol (Andreae and Merlet, 2001;Koch et al., 2009;IPCC, 2014) In most cases, the measurements of aerosol optical properties are either limited to a specific source region or confined to a limited wavelength range. Internally versus externally mixed particles can have very different optical properties (e.g.,(Jacobson, 2000;Stier et al., 2006;Schwarz et al., 2008)). The processing of fire emissions leading to the eventual formation of secondary organic aerosols (SOA) is complex, including dilution, partial evolution of the primary organic aerosols (POA) into gaseous species, photochemical reactions of organic species, partitioning of semi volatile primary emissions into the condensed phase upon cooling, and multiphase chemical conversion (including cloud processing) (Bruns et al., 2016).

Furthermore, it is often wrongly assumed that the only two aerosols to contribute significantly to light absorption on a global scale are black carbon (BC) and mineral dust. Current climate models fail to recognize that organic aerosols (OA) is not purely scattering (Bond et al., 2011;Ma et al., 2012;Bahadur et al., 2012;Laskin et al., 2015). Rather, there is a growing amount of data indicating that a certain class of OA, known as brown carbon (BrC), can be commonly found on a global scale, particularly in urban environments, where it contributes significantly to the total aerosol absorption, specifically in the lower visible and ultraviolet wavelength range, where BC absorbs weakly (Chung et al., 2012;Kirchstetter et al., 2004;Yang et al., 2009;Laskin et al., 2015). Global simulations suggest that this strongly absorbing BrC contributes from +0.12 to +0.25 W m^{-2} or up to 19 % of the absorption by anthropogenic aerosols (Feng et al., 2013;Brown et al., 2018;Saleh et al., 2015;Saleh et al., 2014).

The environmental and health costs of pollutants emitted from open biomass burning and cookstoves are significant and have been associated with human health effects, including early deaths and low infant birth weight. There is a strong evidence for acute respiratory illnesses such as asthma, and chronic obstructive pulmonary disease (COPD) associated with open biomass burning (Naeher et al., 2007;Stefanidou et al., 2008;Holstius et al., 2012;Johnston et al., 2012;Johnston et al., 2011;Elliott et al., 2013;Henderson et al., 2011;Delfino et al., 2009;Rappold et al., 2011;Sutherland et al., 2005;Smith and Pillarisetti, 2017). Wildfire can have health impacts well beyond the perimeter of the fire even thousands of miles downwind (Spracklen et al., 2009).

This work is focused on biomass fuels from east Africa. As of 2019, nine out of ten, or 573 million people in sub-Saharan Africa, will remain without access to electricity by 2030 (Bank, 2019). The African continent is the largest source of BB emissions, with recent studies estimating African contributions to be ~55% of total global emissions of BB aerosols (Ichoku et al., 2008;Roberts et al., 2009;Roberts and Wooster, 2008;Lamarque et al., 2010;van der Werf et al., 2010;Schultz et al., 2008). African combustion emissions are expected to grow. For example, organic carbon emissions from Africa, are expected to make up 50% of the total global emissions in 2030 (Liousse et al., 2014). Africa currently has the fastest growing population in the world; projected to more than double between 2010 and 2050, and surpassing two billion (UN, 2011).

BB is a global phenomenon, and it was shown that the long-range transport of pollutants emitted from BB can affect air quality very far from the source (Edwards et al., 2006;Williams et al., 2012). Although the optical properties of BB aerosols emitted by biomass species native to North America have been extensively investigated

https://doi.org/10.5194/acp-2019-1156
Preprint. Discussion started: 6 February 2020

Atmospheric Chemistry and Physics Discussions

(Hodzic et al., 2007;Yokelson et al., 2009;Liu et al., 2014;McMeeking et al., 2009;Levin et al., 2010;Mack, 2008;Mack et al., 2010), biomass fuels native to sub-Saharan Africa have only been studied during a few field campaigns (Eck et al., 2001;Liousse et al., 2010;Formenti et al., 2003). Due to the very limited available data, the models being used for air quality and climate change in Africa rely on global inventories, which are primarily collected from North America, Europe and Asia (Bond et al., 2004;Streets et al., 2004;Bond et al., 2007;Klimont et al., 2009;Lamarque et al., 2010;Klimont et al., 2013), and are not consistent with satellite observations (Liousse et al., 2010;Malavelle et al., 2011;Liousse et al., 2014) over Africa.

To the author's knowledge, laboratory studies of the optical properties of BB aerosols from solid wood biomass fuels common for domestic use in east Africa have not been conducted. The only other African fuel studied were savannah grass from South Africa during FLAME-4 (Pokhrel et al., 2016) and savannah grass from Namibia and Brachystegia spiciformis from Zimbabwe during the Impact of Vegetation Fires on the Composition and Circulation of the Atmosphere (EFEU) project (Hungershoefer et al., 2008). With the exception of these two examples almost all reported laboratory studies have been focused predominantly on North American fuels (Hodshire et al., 2019). To improve air quality and climate change models for Africa, there is a need for laboratory studies to measure optical properties of BB aerosols from African fuel sources as the aerosols age and interact with polluted air that has the same chemical profile as African megacities and rural areas.

Smog chambers provide a controlled environment for a comprehensive study of aerosol optical properties, chemical and morphological evolution and SOA formation. While fuel specific studies cannot be easily compared to wildfire field studies (Akagi et al., 2012), they can be used to compare emissions from domestic biomass use where the fuel type is known and is often not mixed. It is suggested that burn conditions influence emissions and aerosol mass (Yokelson et al., 2013;Liu et al., 2017) and may be a key difference between laboratory and field studies. In our work, we use a tube furnace for initiating the burn, where we have full control of temperature, airflow, and material combusted. Comparative laboratory studies of BB aerosol optical properties using fuels from Africa and higher latitudes under varying conditions and background pollutant abundances and photochemical aging will provide information on factors most critical for radiative impacts of BB aerosols.

In the first part of his study, we report the results from three biomass fuels from east Africa considered for a systematic fuel-specific study of optical properties of BB aerosols under different aging and burning conditions using an indoor smog chamber. Optical properties were measured for BB aerosols produced under smoldering and flaming conditions for each fuel type. For each burn condition, we report the measured optical properties i.e. scattering and extinction cross sections, single scattering albedo (SSA) for fresh emissions, dark aged, photochemically aged and photochemically aged with added VOC's to represent urban emissions from a representative African megacity.

2 Experimental methods

For this study, authentic fuel plants were obtained from east Africa. These samples were weighed on a calibrated analytical balance so that it would approximately yield a total aerosol loading representative of a scenario (urban, wildfire, etc.). We utilized previously measured emission factors (EFs) (Akagi et al., 2011;Simoneit, 2002;Yokelson et al., 2013;Andreae and Merlet, 2001), such as 18.5±4.1 g PM_{10} kg^{-1} wood (dry weight) for tropical

https://doi.org/10.5194/acp-2019-1156
Preprint. Discussion started: 6 February 2020

Atmospheric Chemistry and Physics Discussions

forest fuels (Akagi et al., 2011). For instance, to achieve a mass loading of 1100 μg m^{-3}, which is the mean loading found in urban/suburban residential locations (Oyem, 2010), 0.5 g of wood was burned in these experiments. These fuel samples were left under a hood to dry out for over a year and were expected to have little to no moisture content.

2.1 BB aerosol generation

For laboratory samples, BB aerosols were generated by combusting wood samples in a tube furnace. This process has been described elsewhere in detail and is summarized here for clarity (Poudel et al., 2017;Smith et al., 2019). Samples with a mass of 0.5 g were typically used for experiments, which generally produces enough BB aerosol for optical property measurements without overloading any of the instruments. Samples as small as 0.1 g and as large as 5 g have been used before, with the maximum mass loading for the tube furnace near 10 g. Biomass samples were placed in a quartz combustion boat (AdValue Technology, FQ-BT-03), which was in turn placed at the center of the working tube inside the furnace (Carbolite Gero, HST120300-120SN). Oxygen content can be varied between ambient conditions and the oxygen-starved conditions found within forest fires by mixing air from a zero-air generator (Aadco Instruments, 747-30) with nitrogen. Flows from both gases are regulated by calibrated mass flow controllers (MFC, Sierra Instruments). For this work, only zero air was used at a flow rate of 10 sL min^{-1}. A furnace temperature of 500 °C was used to represent the smoldering stage of a fire, while 800 °C was used to represent the flaming stage. Although a continuum exists between these two stages, 800 °C was chosen for the flaming stage, since little to no smoldering occurs at this temperature, and the modified combustion efficiency (MCE) value was > 0.98. We could also visually clearly distinguish between brown and black carbon, produced at 500° C and 800° C, respectively, when collected on filter samples.

The North Carolina Agricultural and Technical State University (NCAT) indoor smog chamber has a volume of 9.01 m^3 and is lined by Fluorinated ethylene propylene FEP) Teflon. Two sides each have a bank of 32 ultraviolet (UV) lights (Sylvania, F30T8/350BL/ECO, 36"), for a total of 64 lamps. Emissions from combustion (gas and particles) were transferred to the smog chamber via heated (200° C), ¼ inch stainless steel tubing, after which they undergo cooling and dilution in a natural fashion rather than a stepwise process. A mixing fan was used to produces a well-mixed volume within 10 to 20 minutes after combustion. In these experiments, the fan ran for 10 minutes while smoke was being introduced to the chamber, then for another 10 minutes after the furnace had been disconnected from the chamber. The chamber was constantly diluted by zero air (from generator). The flow rate was varied depending on the sampling demands of instrumentation but was usually around 4 L min^{-1} for a normal cavity ring down spectroscopy (CRDS) experiment.

2.1.1 Burning stages

MCE were calculated from CO and CO_2 measurements. These measurements underwent external calibration with either a pure gas (for CO_2) or a certified standard (199.7 ppm for CO and 5028 ppm for CO_2, purchased from Airgas National Welders). Gas filter correlation analyzers from Thermo Scientific were used to measure CO and CO_2

https://doi.org/10.5194/acp-2019-1156
Preprint. Discussion started: 6 February 2020

Atmospheric Chemistry and Physics Discussions

(models 48C and 41C, respectively). The change in the CO and CO_2 concentration was determined by comparing average measurements before a burn took place, and after the burn, once measurements rose and stabilized. Averages of elevated concentration were taken soon after measurements stabilized, but before dilution could take place. Between 80s and 300s measurements at 10 Hz were averaged for the pre-burn state, and ~300s for the post-burn state. MCE was determined by the following equation:

$$MCE = \frac{\Delta[CO_2]}{\Delta[CO_2]+\Delta[CO]} \quad (1)$$

.

A limitation of open burn experiments performed in large chambers is that the burning efficiency and fuel type are likely coupled (Liu et al., 2014;Pokhrel et al., 2016). To adjust for differences between laboratory and field measurements, relationships were determined for SSA and absorption angstrom exponent (AAE) against MCE or OA/(OA+BC), and SSA and AAE were derived from these relationships using observations of CO, CO_2, OA, and BC.

2.1.2 Indoor smog chamber and characteristics

The smog chamber was constructed to sample several particulate and gas-phase species. Ozone (O_3) was measured with a Thermo- Environmental Instruments UV photometer (model 49), and NO_x was measured with a Monitor Labs fluorescence analyzer (model 8840), The O_3, and NO_x analyzer signals were digitized with a DAQ (National Instruments, USB-6002) and the signal was displayed and stored via custom software (LabVIEW).

Several parameters concerning our chamber itself have already been determined and reported (Smith et al., 2019). Chamber performance is affected by the intensity and spectral character of radiation, surface-to-volume ratio, and nature and condition of the wall surface (Hennigan et al., 2011). For our chamber, wall-loss rates of NO, NO_2, O_3 and PM were determined. Total light intensity was determined in a separate experiment by measuring photolysis of NO_2 and knowing the spectral output of the UV lamps. The wall loss rates for NO, NO_2, and O_3 were found to be $(7.40 \pm 0.01) \times 10^{-4}$, $(3.47 \pm 0.01) \times 10^{-4}$, and $(5.90 \pm 0.08) \times 10^{-4}$ min^{-1}, respectively. The NO_2 photolysis rate constant was 0.165 ± 0.005 min^{-1}, which corresponds to a flux of $(7.72 \pm 0.25) \times 10^{17}$ photons nm cm^{-2} s^{-1} for 296.0 – 516.8 nm, and the particle deposition rate was $(9.46 \pm 0.18) \times 10^{-3}$ min^{-1} for 100 nm mobility diameter BB particles from pine (Smith et al., 2019). Total aerosol surface area peaks approximately 20 minutes after combustion, while total aerosol volume peaks approximately 45 minutes after combustion. The aerosol appears to be well mixed within 20 minutes of combustion, with the size distribution resolving into a single lognormal distribution. However, this distribution continues to shift towards larger particle sizes, even after remaining in the smog chamber for over 24 h. This shift could be due to loss of small particles due to diffusion, coagulation etc. The gas and particle loss rates and other properties for our chamber are comparable to similar indoor smog chambers previously reported e.g. (Babar et al., 2016;Leskinen et al., 2015;Wang et al., 2014;Paulsen et al., 2005)). Chamber pressure and temperature did not vary much from room pressure and temperature during these experiments. Even when the chamber was clearly pressurized, our sensor was not sensitive enough to show a change in pressure.

https://doi.org/10.5194/acp-2019-1156
Preprint. Discussion started: 6 February 2020

Atmospheric Chemistry and Physics Discussions

190

Growth of aerosol particle inside the chamber was represented as a growth in geometric mean diameter (GMD) of the size distribution as shown in Fig. 1. Aerosol growth in the chamber was expected to be due to coagulation of particles and condensation of the gases into existing particles. It is evident from the Fig. 1 that growth
195 is larger for the photochemical aging conditions compared to the dark aging indicating aerosol growth is due to condensation. However, for 800° C combustion, growth in GMD is the same for dark and photochemical aging conditions indicating that there was no condensational growth in those experiments.

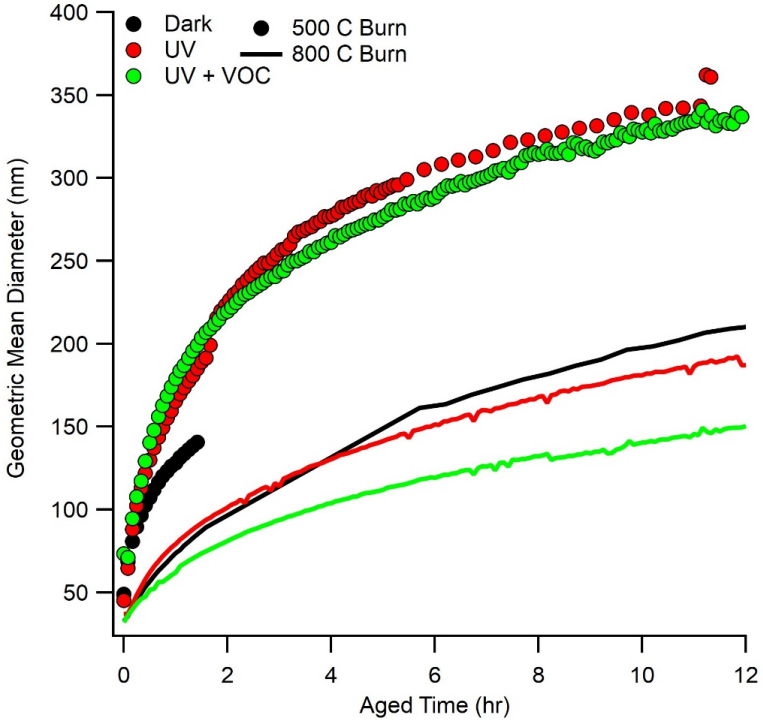

200 **Figure 1**: Growth of geometric mean diameter as a function of photochemical age for eucalyptus under different burn and aged conditions represented in legend (black for dark aging, red for aging under light, and green for aging under light plus VOCs with solid line for 800° C and filled circle for 500° C combustion cases). Except for dark aging conditions, zero time represent the time at which light is turn on.

2.1.3 Chamber cleaning

205

Between experiments, the smog chamber was flushed with zero air (from generator) for a minimum of 24 hours before starting the next experiment. The flow rate was varied somewhat, but was at least 10 L min^{-1} up to usually no more than 20 L min^{-1}. The furnace was also cleaned during this time and is reconnected to the chamber while it is

https://doi.org/10.5194/acp-2019-1156
Preprint. Discussion started: 6 February 2020

still flushing. Even when precautions were taken, this can introduce additional contaminants, which also need to be flushed out before a new burn. This additional flushing can take anywhere from 6 – 24 hours. When the chamber was not needed immediately, flushing continues at a constant 10 L min^{-1} to prevent room air from leaking into the chamber.

2.2 BB aerosol aging

2.2.1 Photochemical aging in a clean environment

For the purposes of these experiments, we define clean environment to be a smog chamber flushed out for 24 hours with clean air coming from the clean air generator. The only VOC's in the chamber come from the combustion of the fuel samples. Optical properties were measured using the procedure described below soon after the chamber was well mixed. The experiments were repeated after keeping the BB aerosol in the chamber overnight (24 hours) without the UV lights. For the photochemical aging, a new burn was made, and the particles were kept in the chamber for 12 hours with the UV lights on.

2.2.2 Photochemical aging in a polluted environment

A high degree of accuracy is required in setting up the conditions of an experiment and performing subsequent measurements. All gas-phase measurements were traceable to an analytical balance (calibrated yearly), NIST-certified flow meter (Mesa Laboratories, model Definer 220, calibrated yearly), NIST-certified stopwatch, and/or certified gas standard. Sample introduction accounted for the NO_x produced from BB itself. Individual hydrocarbons and hydrocarbon mixtures were prepared with the analytical balance. These are typically liquids, purchased at high purity. Mixtures were prepared at the time of use. The concentration in molecules/cm^3 were determined consistently by measuring the mass of syringes before and after injection into the chamber. Using measured chamber pressure and temperature, the concentration in ppmv was estimated. All instruments were typically calibrated at the same time before a round of experimentation. NO and NO_2 were calibrated by passing certified standards through a calibrated MFC and mixing the standard with a calibrated flow of air in a ~30 mL glass mixing ball. Ozone was produced by passing air through an inline O_3 generator (UVP, model 97-0066-01). Using a calibrated NO_x instrument, the O_3 mixing ratio was determined by titrating it with NO to make NO_2. By measuring the O_3 signal, the calibration of O_3, in mV $ppmv^{-1}$, was performed.

To represent a polluted urban environment, we used emission inventory for urban environments from South Africa. This does not necessarily represent the east African emission inventory but this serves as a proxy since this is the only available data to us for the continent. This was obtained from South African Air Quality Information System (SAAQIS). NOx, NO, NO_2, CO, O_3, benzene, toluene, xylene, and ethylbenzene data for several South African Sites (Diepkloof, Kliprivier, Three Rivers, Sharpeville, Zamdela, Thabazimbi, Lephalale, Phalaborwa, and Mokopane) were obtained.

https://doi.org/10.5194/acp-2019-1156
Preprint. Discussion started: 6 February 2020

Atmospheric Chemistry and Physics Discussions

The VOC data was obtained from the two weeks (M-F) of July 11 – 15 and July 18 – 22. These two weeks were in the middle of the peak burning season for South Africa for the year 2016. For the urban area, a ratio of 5:14:6 by concentration (in ppm) for benzene, toluene, and xylene, respectively were used. These concentrations were converted into mass using the volume of the chamber (9010 L), the normal temperature of the chamber (296.64 K), and the normal pressure of the chamber (0.9728 atm). Using the molecular weights of benzene (78.11 g mol^{-1}), toluene (92.14 g mol^{-1}), and xylene (106.17 g mol^{-1}), masses of 0.1406 mg, 0.4645 mg, and 0.8345 mg, respectively were calculated. This was converted into a volume, leading to 0.36 µL for each species, making them equivalent by volume. A mixture was prepared using equal amounts (by volume) of benzene, toluene, and xylene, and was injected by syringe into the U-shaped tube attached to the chamber. This tube was then flushed by zero air into the chamber. The concentration injected into the chamber was approximately 12 times more concentrated than the values found from the emissions data. This was mostly due to ease of sample preparation since the amounts needed for an exact match were too small for our scale to weigh appropriately.

Table 1. Average concentrations (in ppm) of urban emissions for the two weeks of July 11 – 15 and July 18 – 22, 2018. Source South African Air Quality Information System (SAAQIS) The urban summary was used to create a solution of VOCs for use in the smog chamber. Concentrations in the chamber are intentionally higher than atmospheric conditions, to age the BB aerosol faster.

	Urban Summary				**Suburban Summary**		
Diepkloof	Benzene	Toluene	Xylene	**Sebokeng**	Benzene	Toluene	Xylene
Average	1.09	3.95	1.12	Average	2.976	7.874	0.26
Rounded	1	4	1	Rounded	3	8	0.25
Kliprivier	Benzene	Toluene	Xylene	**Three Rivers**	Benzene	Toluene	Xylene
Average	1.23	3.01	1.76	Average	0.698	1.914	0.57
Rounded	1.25	3	1.75	Rounded	0.75	2	0.5
Combined	Benzene	Toluene	Xylene	**Zamdela**	Benzene	Toluene	Xylene
Averaged	1.16	3.48	1.44	Average	1.382	2.283	1.282
Rounded	1.25	3.5	1.5	Rounded	1.5	2.25	1.25
Ratio	5	14	6				
				Combined	Benzene	Toluene	Xylene
				Averaged	1.69	4.02	0.7
				Rounded	1.75	4	0.75
				Ratio	7	16	3

https://doi.org/10.5194/acp-2019-1156
Preprint. Discussion started: 6 February 2020

Atmospheric Chemistry and Physics Discussions

2.3 Optical properties measurement

BB aerosol was size selected for optical property measurements by passing air and particles from the smog chamber through a 710 μm impactor inlet (3.8 μm diameter cut point), neutralizer (TSI model 3081), and a long differential mobility analyzer (DMA) (TSI model 3080). Particles with mobility diameters centered at 200, 300, and 400 nm were selected by the DMA for this study. We verified that the standard deviations of the size distributions didn't overlap (Poudel et al., 2017). Aerosol number density was measured by a water condensation particle counter (WCPC) (TSI model 3788), which was attached after the optical property instruments (shown in Fig. 2) and provided flow through the entire setup at 0.58 sL min^{-1}. Further, the DMA and WCPC could be rearranged and combined to form a scanning mobility particle sizer (SMPS), which was used to determine size distributions before taking optical property measurements.

Optical properties were measured using the extinction-minus-scattering technique (Weingartner et al., 2003;Bond et al., 1999;Sheridan et al., 2005), which uses CRDS to measure the total extinction of light and integrating sphere nephelometry to measure the scattering of light for the same aerosol sample (Moosmüller et al., 2005;Thompson et al., 2002;Thompson et al., 2008;Strawa et al., 2006). The details of the CRDS/Nephelometry optical properties measurement system is described in our recent work (Singh et al., 2014;Singh et al., 2016). A brief description is provided here. The extinction coefficient α_{ext} (m^{-1}) is defined as:

$$\alpha_{ext} = \frac{R_L}{c_{air}}\left(\frac{1}{\tau} - \frac{1}{\tau_0}\right) = \sigma_{ext} N_{CRD} \quad (2)$$

where c_{air} is the speed of light in air and R_L is the ratio of mirror-to-mirror distance d to the length of the cavity occupied by the sample, resulting in a unitless value >1.

After being size selected, aerosol enter the ring-down cavity, where extinction was measured by passing a laser beam coupled to the cavity mode through the sample volume. The 355 nm beam from a Continuum Surelite I-20 Nd:YAG laser (at 20 Hz) pumps an optical parametric oscillator (OPO) laser, which can produce a range of wavelengths. For this study, we used a wavelength range of 500 to 580 nm and a single set of mirrors. Highly reflective mirrors confine most of the laser intensity within the CRDS, with a photomultiplier tube measuring the intensity of the light exiting the mirror after each round trip inside the cavity. Extinction is determined from the decay of light intensity exiting the mirrors. A purge flow of nitrogen was used to keep these mirrors clean. After the CRDS the aerosols enter the integrating nephelometer (TSI, model 3563), where scattering is measured at three wavelengths (centered at 453, 554, and 698 nm) by three different photomultiplier tubes, each of which having a different dichroic filter. Lastly, the number density of the particles was measured by the WCPC, as stated above.

https://doi.org/10.5194/acp-2019-1156
Preprint. Discussion started: 6 February 2020

Atmospheric Chemistry and Physics Discussions

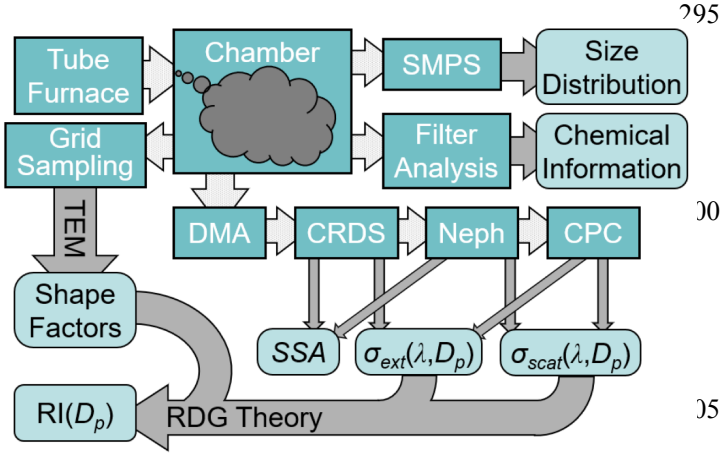

Figure 2. Scheme and flowchart for optical properties measurement

All flows, except the DMA sheath flow, are calibrated against a NIST-certified flow meter (Mesa Laboratories, model Definer 220) that is factory calibrated on a yearly basis and has a listed accuracy of < 1 %. Figure 2 describes the flowchart of the experiments.

2.4 Error analysis of optical properties measurements

In our previous work (Singh et al., 2014) we have comprehensively and holistically accounted for known sources of random and systematic errors and developed a statistical framework for including the contributions to random error. The combined extinction cross section uncertainty (10 – 11%) was largely dominated by CPC measurement error (10%). The calculation flow determining average extinction cross section (σ_{ext}), absorption cross section (σ_{abs}), and single scattering albedo (ω), and their errors was already described (Singh et al., 2014)

The DMA can often allow multiply charged particles to pass through that can show an apparent increase in measured cross sections, even for small number densities (Uin et al., 2011). Other groups have shown that measured extinction coefficients exceeded the predicted ones for 100 and 200 nm particles, which are most affected by the "multiple size–multiple charge" problem (Radney et al., 2009). As such, only particles 200 nm or greater were considered in this work. However, even with 200 nm particles, it has been shown that a small DMA sizing error can still produce significant changes in the extinction (Radney et al., 2013). In principle, errors in the DMA must be corrected (Miles et al., 2011;Toole et al., 2013). However, we did not make corrections due to DMA sizing error in this work.

2.5 Aerosol chemical speciation monitor (ACSM)

An aerosol chemical speciation monitor (ACSM; Aerodyne Research Inc., USA) was used to measure the chemical composition of sub-micron non-refractive particulate mass. Details about the ACSM can be found elsewhere (Ng et al., 2011). Briefly, dry aerosol from the chamber was sampled into the ACSM through a critical aperture with a diameter of 100 µm at a flow rate of 85 mL min^{-1}. The recorded data was processed using the ACSM local toolkit

https://doi.org/10.5194/acp-2019-1156
Preprint. Discussion started: 6 February 2020

Atmospheric Chemistry and Physics Discussions

(v.1.6.0.3) for Igor Pro. Since this work does not use mass loading in a quantitative way, we chose a collection efficiency from one of the species to serve as a representative for all the species.

3 Results and discussion

3.1 Optical properties measurements.

Aerosol optical properties, namely scattering and extinction coefficient for size selected aerosol, were measured for three different east African fuels. The selected fuels (eucalyptus, olive, and acacia) represent the most common trees in east used for domestic use, which contributes to significant aerosol loading. Each fuel was burned at two different combustion temperatures (500^{o}C and 800^{o}C) to investigate the impact of ignition temperature on aerosol optical properties and chemical composition. The optical properties were also measured as a function of different forms of aging: dark aged, photochemically and photochemically aged with added VOC's lights on in the presence of VOCs injected into the chamber before particles were introduced at both temperatures. In this paper, only the results from the combustion at 500^{o}C under all aging conditions and the results of the fresh samples combusted at 800^{o}C are reported. SSA values were measured for some selected particles having mobility diameters of 200, 300 and 400 nm particles.

3.2 Impact of size on SSA

SSA was calculated by taking the ratio of scattering cross-section to the extinction cross-section measured for the wavelength range from 500 − 570 nm at 2.0 nm interval. Calibration of the system and the error analysis in the calculation of SSA from the experimental measurements is described in section 2.3.1. We calculated the scattering coefficients at the CRDS wavelength range by using the scattering angstrom exponent from the measured scattering coefficients.

Sub-micron aerosol shows size dependent SSA values in visible wavelengths. Size selected SSA values estimated in this study are compared with the size selected SSA valued predicted by Mie theory at 532 nm wavelength for both combustion temperature as shown in Figure 3. Refractive indices (real and imaginary parts) were chosen to represent black and brown carbon samples based on values found by Bond and Bergstrom, (2006) and Levin et al. (2010). Figure 3 also shows the SSA of size-selected aerosol from different fuels combusted under different temperatures and the SSA of size-selected aerosol predicted from Mie theory. While no pronounced size dependence was observed for samples combusted at 800^{o}C contrary to what was predicted by Mie theory, the SSA does show size dependence, for samples combusted at 500^{o}C. This may be due to the impact of multiply charged aerosol not discriminated by the DMA. We did not make corrections due to multiply charged particles in this work as described in section 2.3.1. However, the impact of multiply charged particles on SSA is generally small for larger particles considered in this work, which have diameter of 300 or 400 nm. These comparisons are depicted in Fig. 3.

https://doi.org/10.5194/acp-2019-1156
Preprint. Discussion started: 6 February 2020

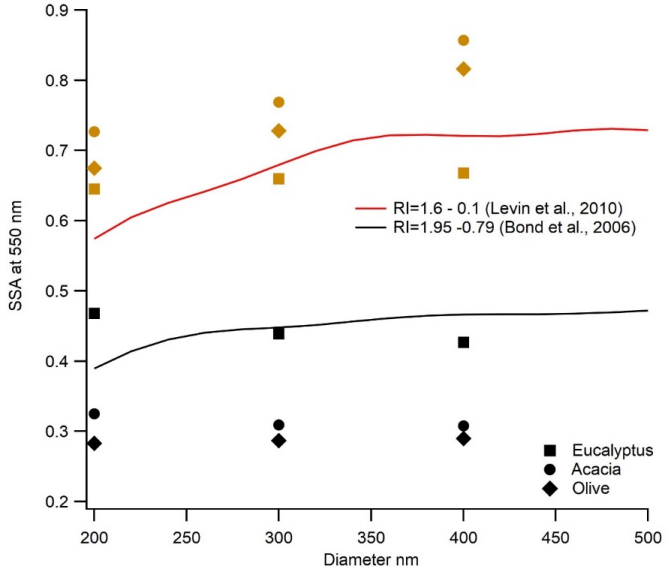

Figure 3: Impact of aerosol particle size on SSA. The solid red line is modeled SSA using Mie theory using refractive index from Levin et al. (2010), representing typical BB emission and black line is modeled SSA by Mie theory using refractive index from Bond et al. (2006), representing black carbon. Symbols are the different fuel types represented in the legend with black color for 800^{o} C burn and brown color for 500^{o} C burn.

.

3.3 Single scattering albedo of freshly emitted aerosol

Figure 4 shows the SSA of freshly emitted 300 nm size aerosol from the different fuels at two different combustion temperatures. The results show no wavelength dependence of SSA in the measured wavelength range of 500-570 nm at both combustion temperatures. However, SSA shows dependence on fuel type even under the same combustion condition. This was consistent for all particle sizes investigated.

https://doi.org/10.5194/acp-2019-1156
Preprint. Discussion started: 6 February 2020

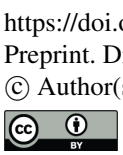

Atmospheric Chemistry and Physics Discussions

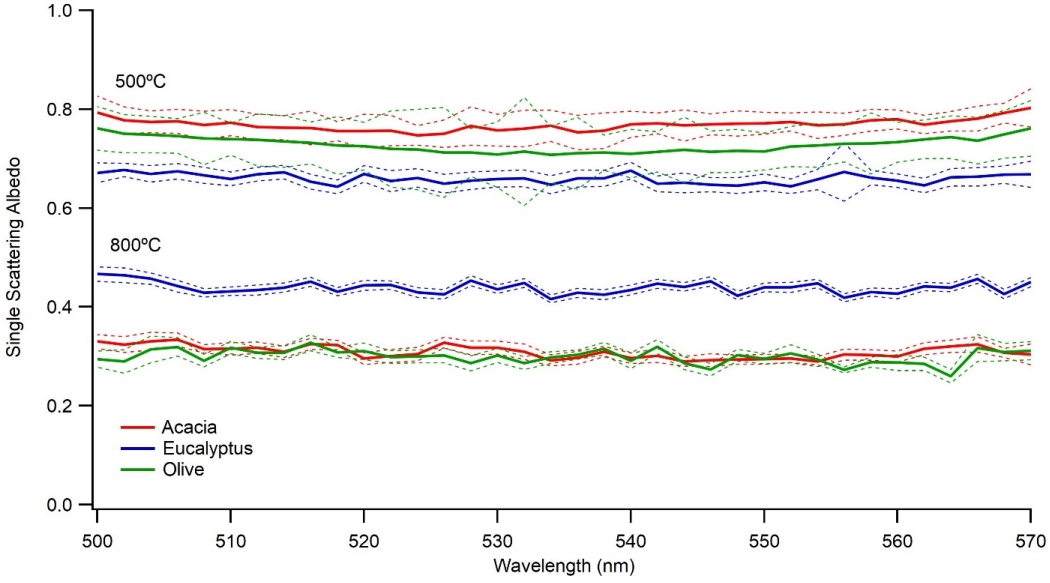

Figure 4: Single scattering albedo of 300 nm size-selected aerosol emitted at combustion temperatures of 500°C and 800°C. Solid blue, green, and red lines are for the average SSA from the three measurements and the dotted lines are the corresponding uncertainties in the measured SSA.

The measured SSA values for 800° C combustions were below 0.5, which indicates highly absorbing aerosol and corresponds to aerosol dominated by black carbon (Pokhrel et al., 2016). The calculated MCE (average from 12 different burns 0.974 ± 0.015) also supports the fact that aerosol emitted from combustion at 800° C represents the flaming stage, which is dominated by BC. The flaming stage of combustion produces more black carbon and less organic carbon (Christian et al., 2003;Ward et al., 1992) which explains the lower values of SSA at visible wavelengths. The impact of combustion temperature on aerosol can be separated visually by looking at the color of the collected filter samples as shown in Fig. S1. As evident from Fig. S1, aerosol emitted from the 800° C combustion looks black whereas that from 500° C combustion looks brownish, indicating a visual difference between black and brown carbon emitted from same fuel under different combustion temperatures. Under the same combustion conditions and airflow, there is a clear but small dependence of SSA on fuel type with eucalyptus producing aerosol with higher SSA than olive and acacia.

While variations in SSA between fuels under similar combustion temperature is relatively small, we observed a large increase in the SSA for samples combusted at 500° C. The range of SSA between different fuels combusted at 800° C is (0.287 to 0.439), whereas the range for of the same fuels combusted at 500° C is (0.66 to 0.769). This indicates that aerosol emissions are dominated by more scattering particles at the lower combustion temperature. This fact is also supported by lower MCE values (averaged from four different burns 0.878 ± 0.008) when combusted at 500° C, where the aerosol is dominated by organic carbon (Christian et al., 2003;Ward et al., 1992). This is consistent with the finding that low temperature biomass burning results in the formation of primary BrC (Bahadur et al., 2012;Lewis

https://doi.org/10.5194/acp-2019-1156
Preprint. Discussion started: 6 February 2020

Atmospheric Chemistry and Physics Discussions

et al., 2008;Radney et al., 2017). Like combustion at 800° C, the SSA depends on fuel type, which might be due to the difference in the chemical compositions of the emitted aerosol. The range of SSA for combustion at 500° C is comparable to previous studies with similar MCE (Liu et al., 2014;Pokhrel et al., 2016). On comparing the SSA of the three different fuels under two different combustion temperatures, it is apparent that SSA is controlled more by the combustion conditions rather than the fuel types. There is a larger variation in SSA for the same fuel under two different combustion conditions compared to the variation due to the inter fuel variability under the same combustion temperature. This result is consistent with the previous study, which showed that SSA is highly correlated with the EC/TC (proxy for the combustion conditions), even for a wide variety of fuels (Pokhrel et al., 2016). A complete list of size-selected SSA of different fuels measured at two combustion temperatures and under different aging conditions is provided in Table S1.

Figure 5 shows the SSA plotted as a function of MCE at 532 nm. Overall, our estimated values of SSA agree well with the previous studies (Pokhrel et al., 2016;Liu et al., 2014) with some outliers. This could potentially be because we are comparing results for size-selected vs bulk aerosols. In general, the variation of the SSA with MCE from the size-selected aerosol show consistent behavior as bulk aerosol with higher SSA for the lower MCE cases and lower SSA for higher MCE cases. This outlier could also be because of the higher error associated with the error higher with the nephelometer, which is responsible for measuring scattering. This could explain why our SSA calculations for BrC was lower than expected. As mentioned earlier, there occur some variabilities in SSA and MCE values even for the same combustion temperature. This could be due the dependence of SSA and MCE on fuel type or due to factors that we are not aware of. In general, however, combustion temperature plays a major role in the optical property of the emitted aerosol. For example, when acacia was burned at 500° C, the SSA was 0.85 ± 0.04 for 400 nm size-selected aerosol, while at 800° C, the SSA was 0.30 ± 0.01. This suggests that by simply varying the combustion temperature, we can generate aerosols with very different optical properties and combustion efficiencies.

https://doi.org/10.5194/acp-2019-1156
Preprint. Discussion started: 6 February 2020

Atmospheric Chemistry and Physics Discussions

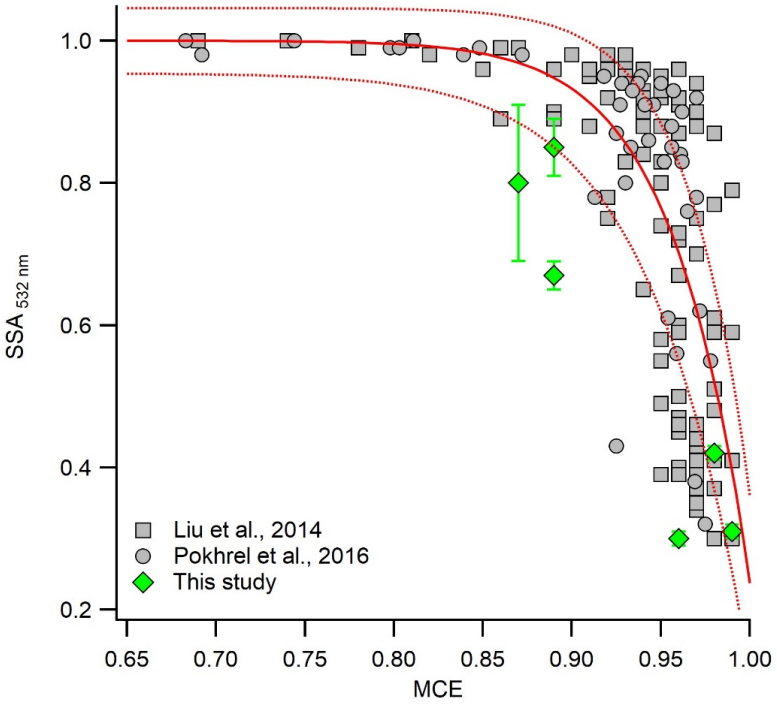

Figure 5: SSA of 400 nm size-selected aerosol at 532 nm as function of MCE under different combustion temperatures. Gray symbols are the SSA of bulk aerosol from previous studies (Liu et al., 2014; Pokhrel et al., 2016). Solid and dashed red lines are the best fit and the uncertainty bounds proposed by Liu et al. (2014)

3.4 Impact of dark aging on SSA

As BB aerosol ages, its properties evolve due to competing chemical and physical processes (Hodshire et al., 2019;Yokelson et al., 2009;Akagi et al., 2012;Vakkari et al., 2018;Formenti et al., 2003;Garofalo et al., 2019) The nighttime atmospheric processes are more complicated as dynamic changes in particle density and size may increase mass loading (Li et al., 2015). Under high relative humidity conditions, heterogeneous reactions may be facilitated to produce more water soluble inorganic salts such as sulfates and nitrites (Shi et al., 2014). The first nighttime field analysis of BB plume intercepts for agricultural fuels showed that oxidation for rice straw and ponderosa pine is dominated by NO_3 (Decker et al., 2019). To simulate the impact of dark aging on aerosol optical properties, BB aerosol was aged without UV lights on and kept overnight for 24 hours. The relative humidity in these experiments was very low (i.e. below the detection limit of our instrument). Optical properties of the freshly emitted aerosol were measured initially, with repeat measurements taken after the particles were left in the chamber to age in the dark. The changes in optical properties is attributed to dark aging. Figure 6 shows the impact of dark aging on SSA for the 300-nm size-selected aerosol emitted during combustion at 500^{o} C. Regardless of fuel type, there occurred an increase in SSA during aging with some fuel dependence, the largest of which was observed for olive. A two-tail T-test confirmed that

https://doi.org/10.5194/acp-2019-1156
Preprint. Discussion started: 6 February 2020

Atmospheric Chemistry and Physics Discussions

increase in mean SSA is statistically significant for all three cases. The results are similar for the 200 nm and 400 nm particles.

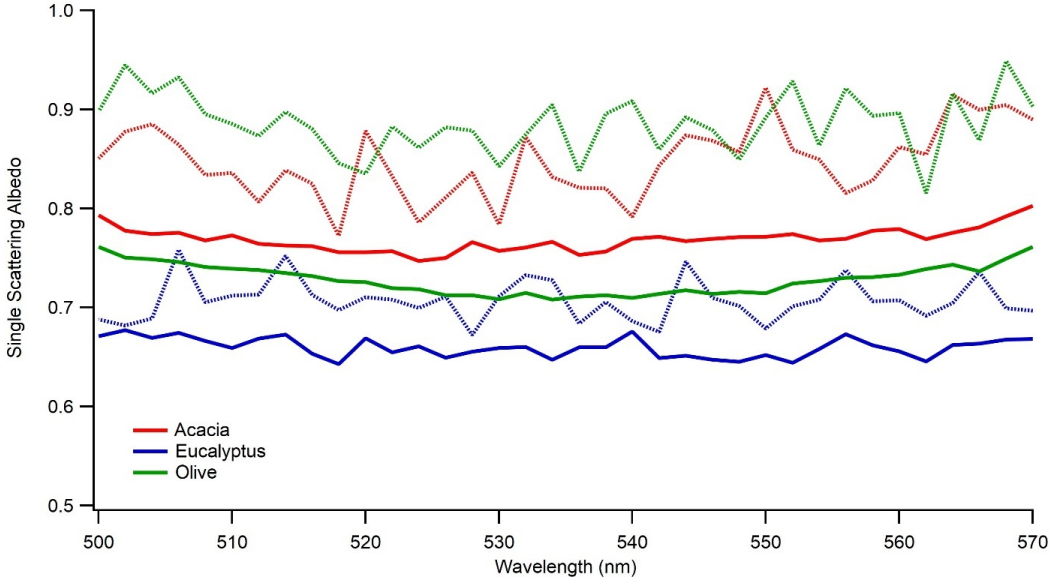

Figure 6: Impact of dark aging on SSA of 300 nm sized-selected aerosol emitted during combustion at 500 °C. Solid lines are for freshly emitted particle and dotted lines are for dark aged particles in the chamber. Different colors are for the different fuels listed in the legend.

Nighttime chemistry in BB studies is still unclear (Hodshire et al., 2019). The potential mechanism for the observed result could be due to nighttime oxidation initiated by ozone or nitrate chemistry or the formation of less/non-absorbing secondary organic aerosol. To further explore the possibility of the observed increase in SSA, we looked at the scattering and extinction cross-section of the fresh and dark aged aerosol. Figure S2 shows the changes in extinction and scattering cross-section of 300 nm size particles emitted during combustion at 500° C under dark aging. For all fuel types studied, there occurred a significant increase in the scattering and extinction cross-section, indicating the occurrence of chemistry, even during dark aging. The increase in cross-section was driven by the scattering cross-section, with no significant change in absorption cross-section during aging. This fact cannot be explained by the heterogeneous chemistry in aerosol phase, because one expects a decrease in absorption cross-section if scattering cross-section of the particle increase. Heterogeneous chemistry is common at high relative humidity (Shi et al., 2014). We hypothesized secondary organic aerosol formation as a potential phenomenon happening during dark aging. It was observed that dark aging produced higher amounts of nitrogen containing organic compounds in the aerosol phase (Li et al., 2015;Ramasamy et al., 2019;Hartikainen et al., 2018) which could be a possible explanation for our experimental results. The fact that the production of non-absorbing secondary organic aerosol will increase the scattering cross-

https://doi.org/10.5194/acp-2019-1156
Preprint. Discussion started: 6 February 2020


Atmospheric Chemistry and Physics Discussions

section of the particles without altering the absorption cross-section explains the observed behaviors in our experiments.

Unlike the 500° C combustion, we were not able to track the aging of aerosol emitted during the 800° C combustion due to some experimental issues. First, there was a significantly low aerosol emission due to more complete combustion of the fuel. For 300 nm and 400 nm size ranges, the number concentration of the particles emitted at 800° C was a factor of two to four lower than those emitted at 500° C. In addition, due to the highly absorbing nature of the aerosol emitted at 800° C, the scattering cross-section of the aerosol was significantly lower than those emitted at 500° C. Therefore, due to the very low number concentration and highly absorbing nature of the particles, the scattering coefficient at 800° C was below the detection limit of our nephelometer during the aging experiments. Hence, we did not feel confident in reporting the SSA of dark aged particles emitted during combustion at 800° C. Figure S3 shows the impact of dark aging on extinction cross-section at 800° C. Even though there occurs significant increase in the extinction cross-sections during dark aging when combusted at 500° C, we did not observe such behaviors during combustion at 800° C, indicating no significant changes in the aerosol optical properties. As shown in Fig. S3 (b), there is a slight increase in the extinction cross-section for olive. However, when accounting a 12 % uncertainty in the cross-section, this increase in extinction cross-section is statistically insignificant. Since extinction cross-section does not change between fresh and dark age of the same aerosol, it can be inferred that there is no change in the SSA during dark aging when combusted at 800° C. This could potentially be due to limited emission of the nighttime oxidants, unlike when combusted at 500° C.

3.5 Impact of photochemical aging

To study the impact of photochemical aging on the optical properties of aerosols, we performed the aging of BB aerosol with the UV light turned on. In addition, to simulate the impact of photochemical aging in a polluted environment, we added VOCs (benzene, toluene, and xylene) to mimic urban pollution as described in section 2.2.1. For both conditions, scattering and extinction coefficients were measured after 12 hours of aging in the chamber. Figure 7 shows the comparison of SSA of fresh and photochemically aged aerosols. As expected, there occurred enhancement in SSA of photochemically aged aerosol. A key point to mention is that fresh and aged SSA are from two different burns and we confirmed that under the same burn conditions the SSA of the same fuels remain within the measurement uncertainties of our instruments. Since this study used size-selected aerosols, the increase in SSA is only possible if the particles became less absorbing because of aging, which could potentially be due to the formation of non-absorbing secondary organic aerosol during photochemical aging. An increase in SSA is possible during photochemical aging due to degradation in brown carbon absorptivity (Sumlin et al., 2017) but the impact of brown carbon on SSA in mid-visible wavelength is small. BrC components undergo photochemical transformations during atmospheric transport, including photobleaching or photoenhancement of their absorption coefficients. For example, the field studies of Forrister et al. (2015) and Selimovic et al. (2018) observed a substantial decay in aerosol UV light absorption in biomass burning plumes corresponding to a half-life of 9 to 15 hours. Recent laboratory and field studies suggested that OH oxidation in the atmosphere may alter optical properties of BrC, leading to absorption enhancement

https://doi.org/10.5194/acp-2019-1156
Preprint. Discussion started: 6 February 2020

Atmospheric Chemistry and Physics Discussions

or bleaching (Schnitzler and Abbatt, 2018;Sumlin et al., 2017;Dasari et al., 2019). However, these studies were made at 375 and 405 nm wavelength of light, while ours were done in the visible range. As evident from Fig. 7, after 12 hours of aging, BB aerosol becomes highly scattering, leading to SSA values of greater than 0.9 in the mid-visible wavelengths, even though fresh BB aerosol were highly absorbing, with SSA below 0.8. We attempted to study the impact of additional VOCs on SSA during aging. However, no distinct effect was observed. This is because we took our measurements after 12 hours of aging, which seems long enough to characterize the impact of the added VOC due to aging in UV. This fact suggests that a more carefully controlled study is needed to accurately simulate the impact of urban pollution on aerosol single scattering albedo.

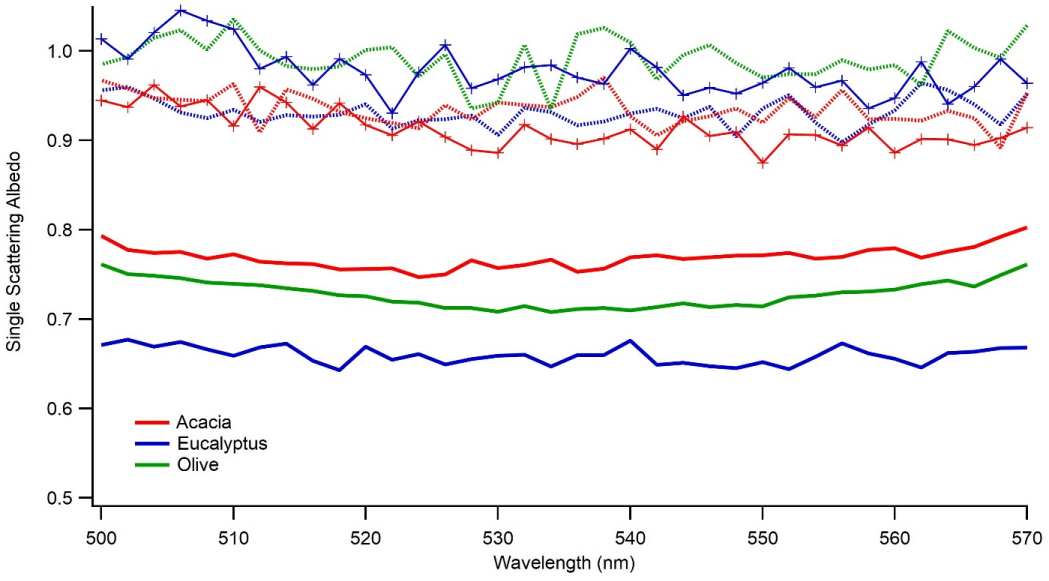

Figure 7: Impact of photochemical aging (light and light plus VOC) on SSA of 300 nm-sized selected aerosols emitted at 500^{o} C combustion. Solid lines are for freshly emitted particles, dotted lines are for aging under the light, and solid lines with symbols are for aging under light plus VOCs. Different colors are for the different fuels listed in the legend.

The impact of the VOCs can be studied by conducting continuous measurement, which is not possible for our setup when the size-selected mode is used. Like dark aged conditions, we were not able to estimate SSA for combustion at 800^{o}C due to the low particle concentration and highly absorbing nature of the aerosol.

During aging, the size distribution of the particles was measured every 5 minutes using SMPS. To account for the impact of additional VOCs on secondary aerosol formation, we estimated the time series of OA enhancement during these experiments. This was done by applying the constant wall loss rate constant as estimated in our previous study (Smith et al., 2019) and assuming a similar loss rate for POA vs SOA. We also assumed that OA is the major aerosol fraction emitted during combustion at 500^{o} C. In addition, we also made an assumption of constant density

https://doi.org/10.5194/acp-2019-1156
Preprint. Discussion started: 6 February 2020

during aging, which gave us the lower estimate of the OA enhancement because as the aerosol aged, the density of the aged aerosol increases compared to POA (Tkacik et al., 2017). The OA enhancement calculation method used in this study was based on the work by Saleh et al. (2013). Briefly, we applied the wall loss time constant to estimate the potential decrease in the OA mass loading only due to wall loss based on the OA mass before the light was turned on. The OA enhancement factor was estimated by taking the ratio of measured aerosol mass with the predicted aerosol mass based on the wall loss rate constant. It is shown that partitioning of vapors to walls in laboratory experiments may alter apparent SOA production (Hodshire et al., 2019). For the particle wall loss rates used in this work, we did not correct for partitioning of vapors to walls, which was not generally negligible (Krechmer et al., 2016). Furthermore, it was shown that the tubing between the tube furnace and smog chamber might create loss and therefore delay the gas phase precursors for SOA formation (Pagonis et al., 2017;Deming et al., 2019;Liu et al., 2019). As described in 2.1, in our set up, combustion emissions passed through a corrugated stainless steel transfer tube. Although relatively short (at 0.5 inches long), passage through this tube increased the loss of BB aerosol between the tube furnace and smog chamber due to the corrugated nature of the tubing. Significant cleaning of this corrugated tube was required between experiments, which indicated that the bulk of the losses between furnace and chamber occurred here. Figure S4 shows the time series of OA enhancement during different aging conditions. We did not observe a distinct difference between the OA enhancement factors under light aged and light plus VOC aged cases. This could potentially be due to our assumptions and the uncertainty related to the SMPS. Previous field and modeling studies found significant enhancement in the SOA formation due to impact of urban pollution (Shrivastava et al., 2019). This fact also suggests that we need more rigorous study to simulate impact of urban pollution of secondary aerosol formation in the laboratory.

Although ACSM was not available early in this study, we designed an experiment to compare the performance of OA enhancement calculation based on the SMPS with the ACSM at a different time. As mentioned earlier, we used a first order decay of the POA based on the estimated wall loss rate constant from the chamber characterization experiments. Figure S5 shows the comparison of OA enhancement using ACSM OA mass loading vs the estimated submicron aerosol mass based on SMPS. In general, the trend of OA enhancement is similar but SMPS seems to underestimate the actual OA enhancement compared to the ACSM. The difference between the OA enhancement estimated by ACSM and SMPS is within 10 %, indicating that estimated OA enhancement lies within the SMPS uncertainty ranges.

4 Conclusions

Biomass burning is the major source of atmospheric primary particles and vapors, which are precursors for secondary aerosols. BB aerosols have been extensively studied through both field and laboratory environments for North American fuels to understand the changes in optical and chemical properties as a function of aging. There is a clear research need for a wider sampling of fuels from different regions of the world for laboratory studies. This work is such an attempt to study the optical and chemical properties of fuels common in east Africa and represents the first such study.

https://doi.org/10.5194/acp-2019-1156
Preprint. Discussion started: 6 February 2020

The existence of significant variability in the observed field and laboratory measurements has been reviewed recently (Hodshire et al., 2019). While laboratory studies provide control over environmental and chemical conditions to study aging by controlling one variable at a time, it may not necessarily recreate atmospheric conditions in atmospheric plumes in the field. Differences in fuel mixture and fuel conditions, such as moisture content, can lead to different emissions. There is a difference in dilution rates between field studies, which is variable, and laboratory studies, which are not variable. Other differences include temperature differences and background OA concentrations. Despite the gap in reconciling field and laboratory studies, some limited comparisons can be made.

For fresh emissions, SSA showed no pronounced size dependence for combustion at 800° C, whereas for combustion at 500° C, some size dependence was observed. This may be due to the impact of multiply charged aerosol, which is not discriminated by the DMA. For the wavelength range used in this study, no wavelength dependence of SSA was observed under all conditions. However, SSA shows dependence on fuel type in general, even under the same combustion conditions.

In general, combustion temperature plays a major role in the optical properties of the emitted aerosol. In all cases the measured SSA values for combustion at 800° C are in the range between 0.287 and 0.439, indicating highly absorbing aerosol, which corresponds to aerosol dominated by black carbon. We observed a large increase in the SSA during combustion at 500° C, which is in the range between 0.66 and 0.769. Under the same combustion conditions and airflow, there is a clear dependence of SSA on fuel type, with eucalyptus producing aerosol with higher SSA than olive and acacia. However, these variations are relatively small, indicating that SSA is more controlled by the combustion conditions than the fuel types.

Regardless of fuel types, there occurred an increase in SSA during dark aging, with some fuel dependence, the largest of which was observed for olive combusted at 500° C. A significant increase in the scattering and extinction cross-section (mostly dominated by scattering) was observed, indicating the occurrence of chemistry, even during dark aging. This fact cannot be explained by the heterogeneous chemistry and hypothesized secondary organic aerosol formation as a potential phenomenon happing during dark aging. This is also consistent with the observed production of nitrogen containing organic compounds during dark aging. The fact that the production of non-absorbing secondary organic aerosol will increase the scattering cross-section of the particles without altering the absorption cross-section explains the observed behaviors in our experiments.

After 12 hours of photochemical aging, BB aerosol becomes highly scattering with SSA values above 0.9, even though fresh emissions were more absorbing with SSA below 0.8. This can be attributed to oxidation in the chamber.

Due to the very low number concertation of aerosols during aging studies of combustion at 800° C, the results were inconclusive, and we plan to conduct measurements by increasing the amount of fuel burned. We also attempted to simulate polluted urban environments by injecting VOCs into the chamber, but no distinct difference was observed, since measurements were done 12 hours after injection of VOCs. No significant OA enhancement was observed because of the VOC injection either, even though significantly enhanced SOA formation was observed in polluted environments. This suggests a need for more rigorous controlled time dependent measurements.

https://doi.org/10.5194/acp-2019-1156
Preprint. Discussion started: 6 February 2020

Atmospheric Chemistry and Physics Discussions

To our knowledge, this is the first laboratory study of optical properties of east African biomass fuels for domestic use. Ongoing work includes systematic study of optical properties using six different African fuels as a function of aging, burn conditions, VOC concertation and RH.

600

Author contribution: Damon Smith conducted the experiments and analyzed the data; Marc Fiddler and Solomon Bililign designed the experiments and contributed to writing and editing. Rudra Pokhrel contributed to the data analysis and interpretation.

605 **Competing interests:** The authors declare that they have no conflict of interest.

610

615

620

625

630

635

https://doi.org/10.5194/acp-2019-1156
Preprint. Discussion started: 6 February 2020

References

Akagi, S. K., Yokelson, R. J., Wiedinmyer, C., Alvarado, M. J., Reid, J. S., Karl, T., Crounse, J. D., and Wennberg, P. O.: Emission Factors for Open and Domestic Biomass Burning for Use in Atmospheric Models, Atmos. Chem. Phys., 11, 4039, 2011.

Akagi, S. K., Craven, J. S., Taylor, J. W., McMeeking, G. R., Yokelson, R. J., Burling, I. R., Urbanski, S. P., Wold, C. E., Seinfeld, J. H., and Coe, H.: Evolution of Trace Gases and Particles Emitted by a Chaparral Fire in California, Atmos. Chem. Phys., 12, 1397, 2012.

Andreae, M. O., and Merlet, P.: Emission of trace gases and aerosols from biomass burning, Global Biogeochemical Cycles, 15, 955-966, 10.1029/2000GB001382, 2001.

Babar, Z. B., Park, J.-H., Kang, J., and Lim, H.-J.: Characterization of a Smog Chamber for Studying Formation and Physicochemical Properties of Secondary Organic Aerosol, Aerosol and Air Quality Research, 16, 3102-3113, 10.4209/aaqr.2015.10.0580, 2016.

Bahadur, R., Praveen, P. S., Xu, Y., and Ramanathan, V.: Solar absorption by elemental and brown carbon determined from spectral observations, Proceedings of the National Academy of Sciences, 109, 17366-17371, 10.1073/pnas.1205910109, 2012.

Bank, W.: More People Have Access to Electricity Than Ever Before, but World Is Falling Short of Sustainable Energy Goals, in, 2019.

Bond, T. C., Anderson, T. L., and Campbell, D.: Calibration and intercomparison of filter-based measurements of visible light absorption by aerosols, Aerosol Science and Technology, 30, 582-600, 10.1080/027868299304435, 1999.

Bond, T. C., Streets, D. G., Yarber, K. F., Nelson, S. M., Woo, J.-H., and Klimont, Z.: A technology-based global inventory of black and organic carbon emissions from combustion, Journal of Geophysical Research: Atmospheres, 109, n/a-n/a, 10.1029/2003JD003697, 2004.

Bond, T. C., Bhardwaj, E., Dong, R., Jogani, R., Jung, S., Roden, C., Streets, D. G., and Trautmann, N. M.: Historical emissions of black and organic carbon aerosol from energy-related combustion, 1850–2000, Global Biogeochemical Cycles, 21, n/a-n/a, 10.1029/2006GB002840, 2007.

Bond, T. C., Zarzycki, C., Flanner, M. G., and Koch, D. M.: Quantifying immediate radiative forcing by black carbon and organic matter with the Specific Forcing Pulse, Atmos. Chem. Phys., 11, 1505-1525, 10.5194/acp-11-1505-2011, 2011.

Boucher, O., D. Randall, P. Artaxo, C. Bretherton, G. Feingold, P. Forster, V.-M. Kerminen, Y. Kondo, H. Liao, U. Lohmann, P. Rasch, S.K. Satheesh, S. Sherwood, B. Stevens and X.Y. Zhang: Clouds and Aerosols, in: Climate Change 2013: The Physical Science Basis. Contribution of Working Group I to the Fifth Assessment Report of the Intergovernmental Panel on Climate Change, edited by: Stocker, T. F., D. Qin, G.-K. Plattner, M. Tignor, S.K. Allen, J. Boschung, A. Nauels, Y. Xia, V. Bex and P.M. Midgley Cambridge University Press, Cambridge, United Kingdom and New York, NY, USA., 2013.

Brown, H., Liu, X., Feng, Y., Jiang, Y., Wu, M., Lu, Z., Wu, C., Murphy, S., and Pokhrel, R.: Radiative effect and climate impacts of brown carbon with the Community Atmosphere Model (CAM5), Atmos. Chem. Phys., 18, 17745-17768, 10.5194/acp-18-17745-2018, 2018.

Bruns, E. A., El Haddad, I., Slowik, J. G., Kilic, D., Klein, F., Baltensperger, U., and Prévôt, A. S. H.: Identification of significant precursor gases of secondary organic aerosols from residential wood combustion, Scientific Reports, 6, 27881, 10.1038/srep27881
https://www.nature.com/articles/srep27881 - supplementary-information, 2016.

https://doi.org/10.5194/acp-2019-1156
Preprint. Discussion started: 6 February 2020

Atmospheric Chemistry and Physics Discussions

690 Christian, T. J., Kleiss, B., Yokelson, R. J., Holzinger, R., Crutzen, P. J., Hao, W. M., Saharjo, B. H., and Ward, D. E.: Comprehensive laboratory measurements of biomass-burning emissions: 1. Emissions from Indonesian, African, and other fuels, Journal of Geophysical Research: Atmospheres, 108, 10.1029/2003jd003704, 2003.

695 Chung, C. E., Ramanathan, V., and Decremer, D.: Observationally constrained estimates of carbonaceous aerosol radiative forcing, Proceedings of the National Academy of Sciences, 109, 11624-11629, 10.1073/pnas.1203707109, 2012.

Crutzen, P., and Andreae, M.: Biomass Burning in the Tropics: Impact on Atmospheric Chemistry and Biogeochemical Cycles, Science (New York, N.Y.), 250, 1669-1678, 10.1126/science.250.4988.1669, 1991.

700

Dasari, S., Andersson, A., Bikkina, S., Holmstrand, H., Budhavant, K., Satheesh, S., Asmi, E., Kesti, J., Backman, J., Salam, A., Bisht, D. S., Tiwari, S., Hameed, Z., and Gustafsson, Ö.: Photochemical degradation affects the light absorption of water-soluble brown carbon in the South Asian outflow, Science Advances, 5, eaau8066, 10.1126/sciadv.aau8066, 2019.

705

Decker, Z. C. J., Zarzana, K. J., Coggon, M., Min, K.-E., Pollack, I., Ryerson, T. B., Peischl, J., Edwards, P., Dubé, W. P., Markovic, M. Z., Roberts, J. M., Veres, P. R., Graus, M., Warneke, C., de Gouw, J., Hatch, L. E., Barsanti, K. C., and Brown, S. S.: Nighttime Chemical Transformation in Biomass Burning Plumes: A Box Model Analysis Initialized with Aircraft Observations, Environmental Science & Technology, 53, 2529-2538, 10.1021/acs.est.8b05359, 2019.

710

Delfino, R. J., Brummel, S., Wu, J., Stern, H., Ostro, B., Lipsett, M., Winer, A., Street, D. H., Zhang, L., Tjoa, T., and Gillen, D. L.: The relationship of respiratory and cardiovascular hospital admissions to the southern California wildfires of 2003, Occupational and Environmental Medicine, 66, 189-197, 10.1136/oem.2008.041376, 2009.

715

Deming, B. L., Pagonis, D., Liu, X., Day, D. A., Talukdar, R., Krechmer, J. E., Gouw, J. A. d., Jimenez, J. L., and Ziemann, P. J.: Measurements of Delays of Gas-Phase Compounds in a Wide Variety of Tubing Materials due to Gas–wall Interactions, Atmos. Meas. Tech., 12, 3453, 2019.

720 Eck, T. F., Holben, B. N., Ward, D. E., Dubovik, O., Reid, J. S., Smirnov, A., Mukelabai, M. M., Hsu, N. C., O'Neill, N. T., and Slutsker, I.: Characterization of the optical properties of biomass burning aerosols in Zambia during the 1997 ZIBBEE field campaign, Journal of Geophysical Research: Atmospheres, 106, 3425-3448, 10.1029/2000JD900555, 2001.

725 Edwards, D. P., Emmons, L. K., Gille, J. C., Chu, A., Attié, J. L., Giglio, L., Wood, S. W., Haywood, J., Deeter, M. N., Massie, S. T., Ziskin, D. C., and Drummond, J. R.: Satellite-observed pollution from Southern Hemisphere biomass burning, Journal of Geophysical Research: Atmospheres, 111, n/a-n/a, 10.1029/2005JD006655, 2006.

730 Elliott, C. T., Henderson, S. B., and Wan, V.: Time series analysis of fine particulate matter and asthma reliever dispensations in populations affected by forest fires, Environmental Health, 12, 11, 10.1186/1476-069X-12-11, 2013.

Feng, Y., Ramanathan, V., and Kotamarthi, V.: Brown carbon: A significant atmospheric absorber of solar radiation, ATMOSPHERIC CHEMISTRY AND PHYSICS, 13, 8607-8621, 10.5194/acp-13-8607-2013, 2013.

735

Formenti, P., Elbert, W., Maenhaut, W., Haywood, J., Osborne, S., and Andreae, M.: Inorganic and carbonaceous aerosols during the Southern African Regional Science Initiative (SAFARI 2000) experiment: Chemical characteristics, physical properties, and emission data for smoke from African biomass burning, Journal of Geophysical Research: Atmospheres, 108, https://doi.org/10.1029/2002jd002408, 2003.

740

Forrister, H., Liu, J., Scheuer, E., Dibb, J., Ziemba, L., Thornhill, K. L., Anderson, B., Diskin, G., Perring, A. E., and Schwarz, J. P.: Evolution of Brown Carbon in Wildfire Plumes, Geophys. Res. Lett., 42, 4623, 2015.

https://doi.org/10.5194/acp-2019-1156
Preprint. Discussion started: 6 February 2020

Atmospheric Chemistry and Physics Discussions

Forster, P., Ramaswamy, V., Artaxo, P., Berntsen, T., Betts, R., Fahey, D., Haywood, J., Lean, J., Lowe, D., Myhre, G., Nganga, J., Prinn, R., Raga, G., Schulz, M., Dorland, R., Bodeker, G., Boucher, O., Collins, W., Conway, T., and Whorf, T.: Changes in Atmospheric Constituents and in Radiative Forcing, in, 2007.

Garofalo, L. A., Pothier, M. A., Levin, E. J. T., Campos, T., Kreidenweis, S. M., and Farmer, D. K.: Emission and Evolution of Submicron Organic Aerosol in Smoke from Wildfires in the Western United States, ACS Earth Space Chem., 3, 1237, 2019.

Hartikainen, A., Yli-Pirilä, P., Tiitta, P., Leskinen, A., Kortelainen, M., Orasche, J., Schnelle-Kreis, J., Lehtinen, K. E. J., Zimmermann, R., Jokiniemi, J., and Sippula, O.: Volatile Organic Compounds from Logwood Combustion: Emissions and Transformation under Dark and Photochemical Aging Conditions in a Smog Chamber, Environmental Science & Technology, 52, 4979-4988, 10.1021/acs.est.7b06269, 2018.

Henderson, S. B., Brauer, M., MacNab, Y. C., and Kennedy, S. M.: Three Measures of Forest Fire Smoke Exposure and Their Associations with Respiratory and Cardiovascular Health Outcomes in a Population-Based Cohort, Environmental Health Perspectives, 119, 1266-1271, doi:10.1289/ehp.1002288, 2011.

Hennigan, C. J., Miracolo, M. A., Engelhart, G. J., May, A. A., Presto, A. A., Lee, T., Sullivan, A. P., McMeeking, G. R., Coe, H., Wold, C. E., Hao, W. M., Gilman, J. B., Kuster, W. C., de Gouw, J., Schichtel, B. A., Collett Jr, J. L., Kreidenweis, S. M., and Robinson, A. L.: Chemical and physical transformations of organic aerosol from the photo-oxidation of open biomass burning emissions in an environmental chamber, Atmos. Chem. Phys., 11, 7669-7686, 10.5194/acp-11-7669-2011, 2011.

Hodshire, A. L., Akherati, A., Alvarado, M. J., Brown-Steiner, B., Jathar, S. H., Jimenez, J. L., Kreidenweis, S. M., Lonsdale, C. R., Onasch, T. B., Ortega, A. M., and Pierce, J. R.: Aging Effects on Biomass Burning Aerosol Mass and Composition: A Critical Review of Field and Laboratory Studies, Environmental Science & Technology, 53, 10007-10022, 10.1021/acs.est.9b02588, 2019.

Hodzic, A., Madronich, S., Bohn, B., Massie, S., Menut, L., and Wiedinmyer, C.: Wildfire particulate matter in Europe during summer 2003: meso-scale modeling of smoke emissions, transport and radiative effects, Atmos. Chem. Phys., 7, 4043-4064, 10.5194/acp-7-4043-2007, 2007.

Holstius, D. M., Reid, C. E., Jesdale, B. M., and Morello-Frosch, R.: Birth Weight following Pregnancy during the 2003 Southern California Wildfires, Environmental Health Perspectives, 120, 1340-1345, doi:10.1289/ehp.1104515, 2012.

Hungershoefer, K., Zeromskiene, K., Iinuma, Y., Helas, G., Trentmann, J., Trautmann, T., Parmar, R., Wiedensohler, A., Andreae, M., and Schmid, O.: Modelling the optical properties of fresh biomass burning aerosol produced in a smoke chamber: results from the EFEU campaign, Atmospheric Chemistry and Physics, 8, 3427-3439, https://doi.org/10.5194/acp-8-3427-2008, 2008.

Ichoku, C., Giglio, L., Wooster, M. J., and Remer, L. A.: Global characterization of biomass-burning patterns using satellite measurements of fire radiative energy, Remote Sensing of Environment, 112, 2950-2962, https://doi.org/10.1016/j.rse.2008.02.009, 2008.

IPCC: IPCC Fifth Assessment Report, Climate Change 2013: The Physical Science Basis, 2014.

Jacobson, M. Z.: A physically-based treatment of elemental carbon optics: Implications for global direct forcing of aerosols, Geophysical Research Letters, 27, 217-220, 10.1029/1999GL010968, 2000.

Johnston, F., Hanigan, I., Henderson, S., Morgan, G., and Bowman, D.: Extreme air pollution events from bushfires and dust storms and their association with mortality in Sydney, Australia 1994–2007, Environmental Research, 111, 811-816, https://doi.org/10.1016/j.envres.2011.05.007, 2011.

https://doi.org/10.5194/acp-2019-1156
Preprint. Discussion started: 6 February 2020

Atmospheric Chemistry and Physics Discussions

Johnston, F. H., Henderson, S. B., Chen, Y., Randerson, J. T., Marlier, M., DeFries, R. S., Kinney, P., Bowman, D. M. J. S., and Brauer, M.: Estimated Global Mortality Attributable to Smoke from Landscape Fires, Environmental Health Perspectives, 120, 695-701, doi:10.1289/ehp.1104422, 2012.

Kirchstetter, T. W., Novakov, T., and Hobbs, P. V.: Evidence that the spectral dependence of light absorption by aerosols is affected by organic carbon, Journal of Geophysical Research: Atmospheres, 109, doi:10.1029/2004JD004999, 2004.

Klimont, Z., Cofala, J., Xing, J., Wei, W., Zhang, C., Wang, S., Kejun, J., Bhandari, P., Mathur, R., Purohit, P., Rafaj, P., Chambers, A., Amann, M., and Hao, J.: Projections of SO2, NOx and carbonaceous aerosols emissions in Asia, Tellus B, 61, 602-617, 10.1111/j.1600-0889.2009.00428.x, 2009.

Klimont, Z., Smith, S. J., and Cofala, J.: The last decade of global anthropogenic sulfur dioxide: 2000–2011 emissions, Environmental Research Letters, 8, 014003, 2013.

Koch, D., Menon, S., Genio, A. D., Ruedy, R., Alienov, I., and Schmidt, G. A.: Distinguishing Aerosol Impacts on Climate over the Past Century, Journal of Climate, 22, 2659-2677, 10.1175/2008jcli2573.1, 2009.

Krechmer, J. E., Pagonis, D., Ziemann, P. J., and Jimenez, J. L.: Quantification of Gas-Wall Partitioning in Teflon Environmental Chambers Using Rapid Bursts of Low-Volatility Oxidized Species Generated in Situ, Environ. Sci. Technol., 50, 5757, 2016.

Lamarque, J. F., Bond, T. C., Eyring, V., Granier, C., Heil, A., Klimont, Z., Lee, D., Liousse, C., Mieville, A., Owen, B., Schultz, M. G., Shindell, D., Smith, S. J., Stehfest, E., Van Aardenne, J., Cooper, O. R., Kainuma, M., Mahowald, N., McConnell, J. R., Naik, V., Riahi, K., and van Vuuren, D. P.: Historical (1850–2000) gridded anthropogenic and biomass burning emissions of reactive gases and aerosols: methodology and application, Atmos. Chem. Phys., 10, 7017-7039, 10.5194/acp-10-7017-2010, 2010.

Laskin, A., Laskin, J., and Nizkorodov, S. A.: Chemistry of atmospheric brown carbon, Chemical reviews, 115, 4335-4382, https://doi.org/10.1029/96jd01512, 2015.

Leskinen, A., Yli-Pirilä, P., Kuuspalo, K., Sippula, O., Jalava, P., Hirvonen, M. R., Jokiniemi, J., Virtanen, A., Komppula, M., and Lehtinen, K. E. J.: Characterization and testing of a new environmental chamber, Atmos. Meas. Tech., 8, 2267-2278, 10.5194/amt-8-2267-2015, 2015.

Levin, E. J. T., McMeeking, G. R., Carrico, C. M., Mack, L. E., Kreidenweis, S. M., Wold, C. E., Moosmüller, H., Arnott, W. P., Hao, W. M., Collett, J. L., and Malm, W. C.: Biomass burning smoke aerosol properties measured during Fire Laboratory at Missoula Experiments (FLAME), Journal of Geophysical Research: Atmospheres, 115, D18210, 10.1029/2009JD013601, 2010.

Lewis, K., Arnott, W. P., Moosmuller, H., and Wold, C. E.: Strong spectral variation of biomass smoke light absorption and single scattering albedo observed with a novel dual-wavelength photoacoustic instrument, J. Geophys. Res., 113, D16203, 2008.

Li, C., Ma, Z., Chen, J., Wang, X., Ye, X., Wang, L., Yang, X., Kan, H., Donaldson, D. J., and Mellouki, A.: Evolution of biomass burning smoke particles in the dark, Atmospheric Environment, 120, 244-252, https://doi.org/10.1016/j.atmosenv.2015.09.003, 2015.

Liousse, C., Guillaume, B., Grégoire, J. M., Mallet, M., Galy, C., Pont, V., Akpo, A., Bedou, M., Castéra, P., Dungall, L., Gardrat, E., Granier, C., Konaré, A., Malavelle, F., Mariscal, A., Mieville, A., Rosset, R., Serça, D., Solmon, F., Tummon, F., Assamoi, E., Yoboué, V., and Van Velthoven, P.: Updated African biomass burning emission inventories in the framework of the AMMA-IDAF program, with an evaluation of combustion aerosols, Atmos. Chem. Phys., 10, 9631-9646, 10.5194/acp-10-9631-2010, 2010.

https://doi.org/10.5194/acp-2019-1156
Preprint. Discussion started: 6 February 2020

Liousse, C., Assamoi, E., Criqui, P., Granier, C., and Rosset, R.: Explosive growth in African combustion emissions from 2005 to 2030, Environmental Research Letters, 9, 035003, https://doi.org/10.1088/1748-9326/9/3/035003, 2014.

Liu, S., Aiken, A. C., Arata, C., Dubey, M. K., Stockwell, C. E., Yokelson, R. J., Stone, E. A., Jayarathne, T., Robinson, A. L., DeMott, P. J., and Kreidenweis, S. M.: Aerosol single scattering albedo dependence on biomass combustion efficiency: Laboratory and field studies, Geophysical Research Letters, 41, 742-748, 10.1002/2013GL058392, 2014.

Liu, X., Huey, L. G., Yokelson, R. J., Selimovic, V., Simpson, I. J., Müller, M., Jimenez, J. L., Campuzano-Jost, P., Beyersdorf, A. J., and Blake, D. R.: Airborne Measurements of Western US Wildfire Emissions: Comparison with Prescribed Burning and Air Quality Implications, J. Geophys. Res. D: Atmos., 122, 6108, 2017.

Liu, X., Deming, B., Pagonis, D., Day, D. A., Palm, B. B., Talukdar, R., Roberts, J. M., Veres, P. R., Krechmer, J. E., Thornton, J. A., de Gouw, J. A., Ziemann, P. J., and Jimenez, J. L.: Effects of gas–wall interactions on measurements of semivolatile compounds and small polar molecules, Atmos. Meas. Tech., 12, 3137-3149, 10.5194/amt-12-3137-2019, 2019.

Ma, X., Yu, F., and Luo, G.: Aerosol direct radiative forcing based on GEOS-Chem-APM and uncertainties, Atmos. Chem. Phys., 12, 5563-5581, 10.5194/acp-12-5563-2012, 2012.

Mack, L. A., Levin, E. J. T., Kreidenweis, S. M., Obrist, D., Moosmüller, H., Lewis, K. A., Arnott, W. P., McMeeking, G. R., Sullivan, A. P., Wold, C. E., Hao, W. M., Collett Jr, J. L., and Malm, W. C.: Optical closure experiments for biomass smoke aerosols, Atmos. Chem. Phys., 10, 9017-9026, 10.5194/acp-10-9017-2010, 2010.

Mack, L. E.: Cavity Ring-Down Sectroscopy and the Retrieval of Aerosol Optical Properties from Biomass Burning During Flame 2, Master's, Colorado State University, CO, USA, 2008.

Malavelle, F., Pont, V., Mallet, M., Solmon, F., Johnson, B., Leon, J.-F., and Liousse, C.: Simulation of aerosol radiative effects over West Africa during DABEX and AMMA SOP-0, Journal of Geophysical Research: Atmospheres, 116, n/a-n/a, 10.1029/2010JD014829, 2011.

McMeeking, G. R., Kreidenweis, S. M., Baker, S., Carrico, C. M., Chow, J. C., Collett, J. L., Hao, W. M., Holden, A. S., Kirchstetter, T. W., Malm, W. C., Moosmüller, H., Sullivan, A. P., and Wold, C. E.: Emissions of trace gases and aerosols during the open combustion of biomass in the laboratory, Journal of Geophysical Research: Atmospheres, 114, D19210, 10.1029/2009JD011836, 2009.

Miles, R. E. H., Rudić, S., Orr-Ewing, A. J., and Reid, J. P.: Sources of Error and Uncertainty in the Use of Cavity Ring Down Spectroscopy to Measure Aerosol Optical Properties, Aerosol Science and Technology, 45, 1360-1375, 10.1080/02786826.2011.596170, 2011.

Moosmüller, H., Varma, R., and Arnott, W. P.: Cavity Ring-Down and Cavity-Enhanced Detection Techniques for the Measurement of Aerosol Extinction, Aerosol Science and Technology, 39, 30-39, 10.1080/027868290903880, 2005.

Naeher, L. P., Brauer, M., Lipsett, M., Zelikoff, J. T., Simpson, C. D., Koenig, J. Q., and Smith, K. R.: Woodsmoke Health Effects: A Review, Inhalation Toxicology, 19, 67-106, 10.1080/08958370600985875, 2007.

Ng, N. L., Herndon, S. C., Trimborn, A., Canagaratna, M. R., Croteau, P. L., Onasch, T. B., Sueper, D., Worsnop, D. R., Zhang, Q., Sun, Y. L., and Jayne, J. T.: An Aerosol Chemical Speciation Monitor (ACSM) for Routine Monitoring of the Composition and Mass Concentrations of Ambient Aerosol, Aerosol Science and Technology, 45, 780-794, 10.1080/02786826.2011.560211, 2011.

Oyem, A. A. a. I., A.F.: Analysis of Atmospheric Aerosol Loading over Nigeria, Environmental Research Journal, 4, 145-156, 2010.

https://doi.org/10.5194/acp-2019-1156
Preprint. Discussion started: 6 February 2020

Pagonis, D., Krechmer, J. E., Gouw, J., Jimenez, J. L., and Ziemann, P. J.: Effects of Gas–wall Partitioning in Teflon Tubing and Instrumentation on Time-Resolved Measurements of Gas-Phase Organic Compounds, Atmos. Meas. Tech., 10, 4687, 2017.

Paulsen, D., Dommen, J., Kalberer, M., Prévôt, A. S. H., Richter, R., Sax, M., Steinbacher, M., Weingartner, E., and Baltensperger, U.: Secondary Organic Aerosol Formation by Irradiation of 1,3,5-Trimethylbenzene−NOx−H2O in a New Reaction Chamber for Atmospheric Chemistry and Physics, Environmental Science & Technology, 39, 2668-2678, 10.1021/es0489137, 2005.

Pokhrel, R. P., Wagner, N. L., Langridge, J. M., Lack, D. A., Jayarathne, T., Stone, E. A., Stockwell, C. E., Yokelson, R. J., and Murphy, S. M.: Parameterization of single-scattering albedo (SSA) and absorption Ångström exponent (AAE) with EC / OC for aerosol emissions from biomass burning, Atmos. Chem. Phys., 16, 9549-9561, 10.5194/acp-16-9549-2016, 2016.

Poudel, S., Fiddler, M., Smith, D., Flurchick, K., and Bililign, S.: Optical properties of biomass burning aerosols: Comparison of experimental measurements and T-Matrix calculations, Atmosphere, 8, 228, https://doi.org/10.3390/atmos8110228, 2017.

Radney, J. G., Bazargan, M. H., Wright, M. E., and Atkinson, D. B.: Laboratory Validation of Aerosol Extinction Coefficient Measurements by a Field-Deployable Pulsed Cavity Ring-Down Transmissometer, Aerosol Science and Technology, 43, 71-80, 10.1080/02786820802482536, 2009.

Radney, J. G., Ma, X., Gillis, K. A., Zachariah, M. R., Hodges, J. T., and Zangmeister, C. D.: Anal. Chem., 85, 8319, 2013.

Radney, J. G., You, R., Zachariah, M. R., and Zangmeister, C. D.: Direct In Situ Mass Specific Absorption Spectra of Biomass Burning Particles Generated from Smoldering Hard and Softwoods, Environmental Science & Technology, 51, 5622-5629, 10.1021/acs.est.7b00810, 2017.

Ramasamy, S., Nakayama, T., Imamura, T., Morino, Y., Kajii, Y., and Sato, K.: Investigation of dark condition nitrate radical- and ozone-initiated aging of toluene secondary organic aerosol: Importance of nitrate radical reactions with phenolic products, Atmospheric Environment, 219, 117049, https://doi.org/10.1016/j.atmosenv.2019.117049, 2019.

Rappold, A. G., Stone, S. L., Cascio, W. E., Neas, L. M., Kilaru, V. J., Carraway, M. S., Szykman, J. J., Ising, A., Cleve, W. E., Meredith, J. T., Vaughan-Batten, H., Deyneka, L., and Devlin, R. B.: Peat Bog Wildfire Smoke Exposure in Rural North Carolina Is Associated with Cardiopulmonary Emergency Department Visits Assessed through Syndromic Surveillance, Environmental Health Perspectives, 119, 1415-1420, doi:10.1289/ehp.1003206, 2011.

Roberts, G., Wooster, M. J., and Lagoudakis, E.: Annual and diurnal african biomass burning temporal dynamics, Biogeosciences, 6, 849-866, 10.5194/bg-6-849-2009, 2009.

Roberts, G. J., and Wooster, M. J.: Fire Detection and Fire Characterization Over Africa Using Meteosat SEVIRI, IEEE Transactions on Geoscience and Remote Sensing, 46, 1200-1218, 10.1109/TGRS.2008.915751, 2008.

Saleh, R., Robinson, E. S., Tkacik, D. S., Ahern, A. T., Liu, S., Aiken, A. C., Sullivan, R. C., Presto, A. A., Dubey, M. K., Yokelson, R. J., Donahue, N. M., and Robinson, A. L.: Brownness of organics in aerosols from biomass burning linked to their black carbon content, Nature Geoscience, 7, 647-650, 10.1038/ngeo2220, 2014.

Saleh, R., Marks, M., Heo, J., Adams, P. J., Donahue, N. M., and Robinson, A. L.: Contribution of brown carbon and lensing to the direct radiative effect of carbonaceous aerosols from biomass and biofuel burning emissions, Journal of Geophysical Research: Atmospheres, 120, 10,285-210,296, 10.1002/2015jd023697, 2015.

Schnitzler, E. G., and Abbatt, J. P. D.: Heterogeneous OH oxidation of secondary brown carbon aerosol, Atmos. Chem. Phys., 18, 14539-14553, 10.5194/acp-18-14539-2018, 2018.

https://doi.org/10.5194/acp-2019-1156
Preprint. Discussion started: 6 February 2020

Atmospheric Chemistry and Physics Discussions

Schultz, M. G., Heil, A., Hoelzemann, J. J., Spessa, A., Thonicke, K., Goldammer, J. G., Held, A. C., Pereira, J. M. C., and van het Bolscher, M.: Global wildland fire emissions from 1960 to 2000, Global Biogeochemical Cycles, 22, GB2002, 10.1029/2007GB003031, 2008.

Schwarz, J. P., Spackman, J. R., Fahey, D. W., Gao, R. S., Lohmann, U., Stier, P., Watts, L. A., Thomson, D. S., Lack, D. A., Pfister, L., Mahoney, M. J., Baumgardner, D., Wilson, J. C., and Reeves, J. M.: Coatings and their enhancement of black carbon light absorption in the tropical atmosphere, Journal of Geophysical Research: Atmospheres, 113, n/a-n/a, 10.1029/2007JD009042, 2008.

Selimovic, V., Yokelson, R. J., Warneke, C., Roberts, J. M., Gouw, J., Reardon, J., and Griffith, D. W. T.: Aerosol Optical Properties and Trace Gas Emissions by PAX and OP-FTIR for Laboratory-Simulated Western US Wildfires during FIREX, Atmos. Chem. Phys., 18, 2929, 2018.

Sheridan, P. J., Arnott, W. P., Ogren, J. A., Andrews, E., Atkinson, D. B., Covert, D. S., Moosmuller, H., Petzold, A., Schmid, B., Strawa, A. W., Varma, R., and Virkkula, A.: The Reno Aerosol Optics Study: An evaluation of aerosol absorption measurement methods, Aerosol Science and Technology, 39, 1-16, 10.1080/027868290901891, 2005.

Shi, Y., Chen, J., Hu, D., Wang, L., Yang, X., and Wang, X.: Airborne submicron particulate (PM1) pollution in Shanghai, China: Chemical variability, formation/dissociation of associated semi-volatile components and the impacts on visibility, Science of The Total Environment, 473-474, 199-206, https://doi.org/10.1016/j.scitotenv.2013.12.024, 2014.

Shrivastava, M., Andreae, M. O., Artaxo, P., Barbosa, H. M. J., Berg, L. K., Brito, J., Ching, J., Easter, R. C., Fan, J., Fast, J. D., Feng, Z., Fuentes, J. D., Glasius, M., Goldstein, A. H., Alves, E. G., Gomes, H., Gu, D., Guenther, A., Jathar, S. H., Kim, S., Liu, Y., Lou, S., Martin, S. T., McNeill, V. F., Medeiros, A., de Sá, S. S., Shilling, J. E., Springston, S. R., Souza, R. A. F., Thornton, J. A., Isaacman-VanWertz, G., Yee, L. D., Ynoue, R., Zaveri, R. A., Zelenyuk, A., and Zhao, C.: Urban pollution greatly enhances formation of natural aerosols over the Amazon rainforest, Nature Communications, 10, 1046, 10.1038/s41467-019-08909-4, 2019.

Simoneit, B. R. T.: Biomass burning — a review of organic tracers for smoke from incomplete combustion, Applied Geochemistry, 17, 129-162, https://doi.org/10.1016/S0883-2927(01)00061-0, 2002.

Singh, S., Fiddler, M. N., Smith, D., and Bililign, S.: Error analysis and uncertainty in the determination of aerosol optical properties using cavity ring-down spectroscopy, integrating nephelometry, and the extinction-minus-scattering method, Aerosol Science and Technology, 48, 1345-1359, https://doi.org/10.1080/02786826.2014.984062, 2014.

Singh, S., Fiddler, M. N., and Bililign, S.: Measurement of size-dependent single scattering albedo of fresh biomass burning aerosols using the extinction-minus-scattering technique with a combination of cavity ring-down spectroscopy and nephelometry, Atmos. Chem. Phys., 16, 13491-13507, 10.5194/acp-16-13491-2016, 2016.

Smith, D. M., Fiddler, M. N., Sexton, K. G., and Bililign, S.: Construction and Characterization of an Indoor Smog Chamber for Measuring the Optical and Physicochemical Properties of Aging Biomass Burning Aerosols, Aerosol and Air Quality Research, 19, 467-483, 10.4209/aaqr.2018.06.0243, 2019.

Smith, K. R., and Pillarisetti, A.: Household Air Pollution from Solid Cookfuels and Its Effects on Health., in: Injury Prevention and Environmental Health. 3rd edition, edited by: CN, M., Nugent R, and O, K., The International Bank for Reconstruction and Development / The World Bank;, Washington (DC), 2017.

Spracklen, D. V., Mickley, L. J., Logan, J. A., Hudman, R. C., Yevich, R., Flannigan, M. D., and Westerling, A. L.: Impacts of climate change from 2000 to 2050 on wildfire activity and carbonaceous aerosol concentrations in the western United States, Journal of Geophysical Research: Atmospheres, 114, 10.1029/2008jd010966, 2009.

Stefanidou, M., Athanaselis, S., and Spiliopoulou, C.: Health Impacts of Fire Smoke Inhalation, Inhalation Toxicology, 20, 761-766, 10.1080/08958370801975311, 2008.

https://doi.org/10.5194/acp-2019-1156
Preprint. Discussion started: 6 February 2020

Stier, P., Seinfeld, J. H., Kinne, S., Feichter, J., and Boucher, O.: Impact of nonabsorbing anthropogenic aerosols on clear-sky atmospheric absorption, Journal of Geophysical Research: Atmospheres, 111, n/a-n/a, 10.1029/2006JD007147, 2006.

Strawa, A. W., Elleman, R., Hallar, A. G., Covert, D., Ricci, K., Provencal, R., Owano, T. W., Jonsson, H. H., Schmid, B., Luu, A. P., Bokarius, K., and Andrews, E.: Comparison of in situ aerosol extinction and scattering coefficient measurements made during the Aerosol Intensive Operating Period, Journal of Geophysical Research: Atmospheres, 111, n/a-n/a, 10.1029/2005JD006056, 2006.

Streets, D. G., Bond, T. C., Lee, T., and Jang, C.: On the future of carbonaceous aerosol emissions, Journal of Geophysical Research: Atmospheres, 109, n/a-n/a, 10.1029/2004JD004902, 2004.

Sumlin, B. J., Pandey, A., Walker, M. J., Pattison, R. S., Williams, B. J., and Chakrabarty, R. K.: Atmospheric Photooxidation Diminishes Light Absorption by Primary Brown Carbon Aerosol from Biomass Burning, Environmental Science & Technology Letters, 4, 540-545, 10.1021/acs.estlett.7b00393, 2017.

Sutherland, E. R., Make, B. J., Vedal, S., Zhang, L., Dutton, S. J., Murphy, J. R., and Silkoff, P. E.: Wildfire smoke and respiratory symptoms in patients with chronic obstructive pulmonary disease, Journal of Allergy and Clinical Immunology, 115, 420-422, 10.1016/j.jaci.2004.11.030, 2005.

Thompson, J. E., Smith, B. W., and Winefordner, J. D.: Monitoring Atmospheric Particulate Matter through Cavity Ring-Down Spectroscopy, Analytical Chemistry, 74, 1962-1967, 10.1021/ac0110505, 2002.

Thompson, J. E., Barta, N., Policarpio, D., and DuVall, R.: A fixed frequency aerosol albedometer, Opt. Express, 16, 2191-2205, 10.1364/OE.16.002191, 2008.

Tkacik, D. S., Robinson, E. S., Ahern, A., Saleh, R., Stockwell, C., Veres, P., Simpson, I. J., Meinardi, S., Blake, D. R., and Yokelson, R. J.: A Dual-Chamber Method for Quantifying the Effects of Atmospheric Perturbations on Secondary Organic Aerosol Formation from Biomass Burning Emissions: Investigation of Biomass Burning SOA, J. Geophys. Res. D: Atmos., 122, 6043, 2017.

Toole, J. R., Renbaum-Wolff, L., and Smith, G. D.: A Calibration Technique for Improving Refractive Index Retrieval from Aerosol Cavity Ring-Down Spectroscopy, Aerosol Science and Technology, 47, 955-965, 10.1080/02786826.2013.805875, 2013.

Uin, J., Tamm, E., and Mirme, A.: Very Long DMA for the Generation of the Calibration Aerosols in Particle Diameter Range up to 10 µm by Electrical Separation, Aerosol and Air Quality Research, 11, 531-538, 10.4209/aaqr.2011.05.0068, 2011.

UN: World Population Prospects: The 2010 Revision, Comprehensive Tables. ST/ESA/SER.A/313., United Nations, Department of Economic and Social Affairs, Population Division, 2011.

Vakkari, V., Beukes, J. P., Dal Maso, M., Aurela, M., Josipovic, M., and van Zyl, P. G.: Major Secondary Aerosol Formation in Southern African Open Biomass Burning Plumes, Nat. Geosci., 11, 580, 2018.

van der Werf, G. R., Randerson, J. T., Giglio, L., Collatz, G. J., Mu, M., Kasibhatla, P. S., Morton, D. C., DeFries, R. S., Jin, Y., and van Leeuwen, T. T.: Global fire emissions and the contribution of deforestation, savanna, forest, agricultural, and peat fires (1997–2009), Atmos. Chem. Phys., 10, 11707-11735, 10.5194/acp-10-11707-2010, 2010.
Wang, X., Liu, T., Bernard, F., Ding, X., Wen, S., Zhang, Y., Zhang, Z., He, Q., Lü, S., Chen, J., Saunders, S., and Yu, J.: Design and characterization of a smog chamber for studying gas-phase chemical mechanisms and aerosol formation, Atmos. Meas. Tech., 7, 301-313, 10.5194/amt-7-301-2014, 2014.

Ward, D. E., Susott, R. A., Kauffman, J. B., Babbitt, R. E., Cummings, D. L., Dias, B., Holben, B. N., Kaufman, Y. J., Rasmussen, R. A., and Setzer, A. W.: Smoke and fire characteristics for cerrado and deforestation burns in Brazil: BASE-B Experiment, Journal of Geophysical Research: Atmospheres, 97, 14601-14619, 10.1029/92jd01218, 1992.

https://doi.org/10.5194/acp-2019-1156
Preprint. Discussion started: 6 February 2020

Atmospheric Chemistry and Physics Discussions

Weingartner, E., Saathoff, H., Schnaiter, M., Streit, N., Bitnar, B., and Baltensperger, U.: Absorption of light by soot particles: Determination of the absorption coefficient by means of aethalometers, Journal of Aerosol Science, 34, 1445-1463, 10.1016/s0021-8502(03)00359-8, 2003.

Williams, J. E., Weele, M. v., Velthoven, P. F. J. v., Scheele, M. P., Liousse, C., and Werf, G. R. v. d.: The Impact of Uncertainties in African Biomass Burning Emission Estimates on Modeling Global Air Quality, Long Range Transport and Tropospheric Chemical Lifetimes, Atmosphere, 3, 132, 2012.

Yang, M., Howell, S. G., Zhuang, J., and Huebert, B. J.: Attribution of aerosol light absorption to black carbon, brown carbon, and dust in China – interpretations of atmospheric measurements during EAST-AIRE, Atmos. Chem. Phys., 9, 2035-2050, 10.5194/acp-9-2035-2009, 2009.

Yokelson, R. J., Crounse, J. D., DeCarlo, P. F., Karl, T., Urbanski, S., Atlas, E., Campos, T., Shinozuka, Y., Kapustin, V., Clarke, A. D., Weinheimer, A., Knapp, D. J., Montzka, D. D., Holloway, J., Weibring, P., Flocke, F., Zheng, W., Toohey, D., Wennberg, P. O., Wiedinmyer, C., Mauldin, L., Fried, A., Richter, D., Walega, J., Jimenez, J. L., Adachi, K., Buseck, P. R., Hall, S. R., and Shetter, R.: Emissions from biomass burning in the Yucatan, Atmos. Chem. Phys., 9, 5785-5812, 10.5194/acp-9-5785-2009, 2009.

Yokelson, R. J., Burling, I. R., Gilman, J. B., Warneke, C., Stockwell, C. E., de Gouw, J., Akagi, S. K., Urbanski, S. P., Veres, P., Roberts, J. M., Kuster, W. C., Reardon, J., Griffith, D. W. T., Johnson, T. J., Hosseini, S., Miller, J. W., Cocker Iii, D. R., Jung, H., and Weise, D. R.: Coupling field and laboratory measurements to estimate the emission factors of identified and unidentified trace gases for prescribed fires, Atmos. Chem. Phys., 13, 89-116, 10.5194/acp-13-89-2013, 2013.